Determining chloride content profiles in concrete using an electrical resistivity tomography device

Milia Fares, Géraldine Villain, Stéphanie Bonnet, Sergio Palma-Lopes, Benoit Thauvin, Mickaël Thiery

Please cite the published version in CCC, 2018, https://doi.org/10.1016/j.cemconcomp.2018.08.001

Determining chloride content profiles in concrete using an Electrical Resistivity Tomography device

Milia FARES[1], Géraldine VILLAIN[1], Stéphanie BONNET[2], Sérgio PALMA LOPES[1], Benoit THAUVIN[3], Mickaël THIERY[4].

[1] IFSTTAR, Centre de Nantes, Allée des Ponts et Chaussées, CS 5004, 44344 Bouguenais, France
miliafares@hotmail.com, geraldine.villain@ifsttar.fr, sergio.lopes@ifsttar.fr
[2] UBL, Université de Nantes, GeM, Institut de Recherche en Génie civil et Mécanique, 52 rue Michel Ange, BP 420, 44 606 Saint-Nazaire, France
stephanie.bonnet@univ-nantes.fr
[3] CEREMA DTER Ouest, Département Laboratoire de St-Brieuc, France
benoit.thauvin@cerema.fr
[4] Ministère de la Transition Ecologique et Solidaire, MTES – MCT / DGALN / DMUP
mickael.thiery@developpement-durable.gouv.fr

Abstract:

Chloride penetration in concrete can lead to steel corrosion which is one of the major pathologies affecting reinforced concrete's durability. The development of methods to investigate chloride penetration is essential to predict and update the service life of the structure. A non-destructive (ND) DC-electrical technique is used in this study: this Electrical Resistivity Tomography (ERT) device is arranged in a Wenner configuration and measures apparent resistivities. Apparent resistivities are then inverted in order to obtain a resistivity profile versus depth. In parallel, a calibration method relating the resistivity to the chloride content for each type of concrete is used to obtain the chloride profile versus depth. This methodology was applied to a chloride diffusion experimental program on two concrete formulations and one mortar. The profiles evaluated by NDT are then compared to those obtained by a destructive method (potentiometric titration). Both types of profile fit relatively well, thus, the presented methodology is validated for determining chloride content profiles by means of a non-destructive ERT device. The evaluation of the uncertainty range of successive processes (measurement, inversion and calibration) underlines the importance on including the uncertainties in the interpretation of the ND profiles in future research.

Keywords: Resistivity, chloride, NDT, diffusion, concrete durability

1. Introduction:

The deterioration of reinforced concrete structures in marine environment is mainly due to the corrosion of steel induced by the penetration of chloride ions [1]. Chloride ions can penetrate into concrete through multiple mechanisms including diffusion, adsorption, permeation and surface deposit of airborne salts [2-7]. By penetrating into the cover concrete, the chloride ions destroy the passive layer that protects the reinforcing steel bars from corrosion. The corrosion mechanism induces a reduction of the steel surface area and rust production on the bars resulting in an increase of the total volume up to 600% [8, 9]. The consequences then

include the decrease of the mechanical resistance of the structure as well as the cracking and the spalling of the concrete.

The duration preceding the destruction of the passive layer is defined according to Tuutti [10] as the initiation period which is followed by the propagation period during which the corrosion develops. The work presented in this paper is positioned in the framework of the inspection of concrete structures in marine environment during this initiation period.

Determining the chloride concentration at the depth of the steel bars allows evaluating the corrosion risks (studies claim a free chloride threshold varying between 0,07 and 1,16% by weight of binder [11]). Before reaching the critical chloride threshold, the monitoring of the evolution of chloride profile permits the assessment of maintenance needs and repair action scheduling [1, 4, 8]. Moreover, the monitoring of the evolution of the chloride profiles allows the update of the service life prediction models of the structures.

Therefore, it is important to determine the chloride concentration profiles and not only to detect the presence of chloride ions or to assess the chloride concentration at only a given depth. This study deals with determining the chloride concentration profiles in cover concrete versus depth using a non-destructive method applied to the concrete surface.

Among the few testing techniques used to determine chloride concentration most are destructive, fastidious and time-consuming [12]. One of the main disadvantages of destructives techniques lies in the fact that by destroying the sample, it is not possible to monitor the evolution of the chloride concentration with time at the same position. Hence, the development of fast and reliable non-destructive methods becomes a necessity.

With non-destructive methods, the rapidity of the measurement makes it possible to investigate a large surface area of the structure and therefore to detect weak points that need further investigation [13, 14]. In addition, being non-invasive, the methods allow surveying the same spot in the structure and assessing the concrete conditions at several test times. The monitoring parameters provided are valuable to predict the potential evolution of the concrete conditions with time.

Amongst non-destructive methods, electromagnetic techniques are particularly sensitive to the moisture and ionic contents in concrete [15-22]. This sensitivity has been proven in lab controlled conditions as well as on in-situ structures [23-25]. More specifically, the DC-electrical resistivity (Ω.m) of concrete is a bulk material property that quantifies the electrical

resistance (applied voltage divided by transmitted current intensity) of a unit volume of concrete.

In concrete, electrical current is carried by the ions present in the pore solution [26]. The resistivity thus depends on the concrete composition (affecting the porosity and tortuosity), on the saturation degree and on the ionic content of the pore solution [20, 27-34]. Concerning the concrete composition, [32] have demonstrated that resistivity increases when the W/C ratio of the studied concrete decreases and therefore when porosity decreases. A similar trend is observed by [35] after measuring concrete specimens with different water to binder ratios. Developed resistivity instruments used on concrete include embedded sensors [36,37] as well as surface applied devices [18].Concerning the saturation degree and the ionic content, although the use of DC-electrical resistivity measurements to assess moisture and ionic contents is fairly common in the fields near-surface geophysics applied to soil science (e.g. [38]), and hydrological or environmental studies (e.g. [39]), approaches are less advanced in the field of concrete durability evaluation.

Recent studies [18, 40] have proven the potential of resistivity techniques to monitor water and chloride ingress in concrete by using electrical resistivity measurements. In [18] the authors compare the potential of three electromagnetic (EM) NDT techniques (electrical resistivity tomography (ERT), capacimetry, and ground-penetrating radar) to monitor water and chloride ingress into cover concrete and point out that separating the influences of both parameters (moisture and chloride contents) in non-saturated concrete would imply a more sophisticated and combined EM approach. In [31] the authors focused on evaluating the detection threshold of chlorides in cover concrete by means of an embedded DC-electrical resistivity probe (for monitoring purposes) and based on statistical analysis and quality assessment approaches. Nevertheless, none of these studies are able to quantify the degree of saturation or the chloride content because the calibration phase is missing. In particular, Du Plooy et al. [18] could not decorrelate the effect of the chloride content from the water saturation profile during a sea water imbibition process, on the apparent resistivities measured by the ERT device.

For a given cement type, a given concrete mix design, and for a zero chloride concentration, a variation in resistivity most likely indicates a variation of the concrete saturation degree. In the same way, for a given cement type, a given concrete mix design, and for a constant saturation degree equal to 100%, a variation in resistivity most likely indicates a variation of the chloride concentration.

It is worth noting that this study deals with chloride diffusion in saturated concrete (S = 100%) with the only variant being therefore the chloride content. Although the rate of chloride penetration in non-saturated conditions is more important and is found in various field situations, separating the two parameters is essential at first given that the resistivity is sensitive to both parameters.

In this paper, we investigate the use of electrical resistivity tomography (ERT) to obtain a chloride profile concentration using the ERT device developed by [41], by means of one-dimension (1D) inversion of raw resistivity data (as opposed to [41] who used a 2D inversion procedure that is somewhat unnecessary for yielding 1D profiles) in addition to material calibration. The article first gives a detailed description of the proposed methodology to obtain chloride content profiles using non-destructive surface measurements. The methodology is validated with an experimental program carried out on three different materials and the results are compared to those obtained by a destructive method.

2. Proposed methodology and experimental measurement methods

As previous studies [18, 40] did not succeed in determining the chloride profiles by ERT, the innovative methodology described in this section is necessary.

2.1 Global methodology to obtain chloride profiles using NDT, including methodology steps

Five main steps can be identified in the process of obtaining a chloride content profile using resistivity measurements (illustrated in Figure 1).

The first step is the measurement of a set of apparent resistivities (ρ_a) on the studied structure using an ERT device (defined in section 2.2.2). Apparent resistivities are the electrical responses of a given material. Each apparent resistivity is obtained by multiplying a measured electrical resistance in Ohms (ratio between the generated potential drop and the corresponding applied current intensity) by a geometric factor (in meters) that accounts for the measurement geometry (see 2.2.2).

For a homogeneous and isotropic material, the apparent resistivities theoretically equal the bulk resistivity of the material. In non-homogeneous materials, each apparent resistivity is an integrated value over a certain volume that depends on the respective measurement geometry. An inversion procedure has to be carried out in order to yield the ‘true’ resistivity distribution [41, 42]. Therefore, the second step is the inversion of the measured apparent resistivities to

obtain a resistivity profile versus depth. The inversion was carried out using the free Res1D software (released for academic use) as will be described in section 2.3.

Parallel to this procedure, the third step entails the measurement of the resistivity of several cores of the same concrete saturated with different concentrations of sodium chloride using the calibration resistivity cell (section 2.2.1): this step is to establish the calibration curves corresponding to the resistivity versus the free chloride content. The free chloride content in concrete was determined by the destructive method described in section 2.4. The calibration is, for the time being at least, a necessary tool in order to convert the resistivity profile obtained in step 2 into chloride concentration profile (step 4). The last step deals with transforming the resistivity profile (step 2) to chloride content profile using the calibration curves obtained with step 3. The propagation of uncertainty throughout the different steps listed above has a considerable impact on the final results as will be detailed in section 4.3.

To validate the chloride profiles obtained in step 4, these are compared with those obtained by the destructive method described in section 2.4.

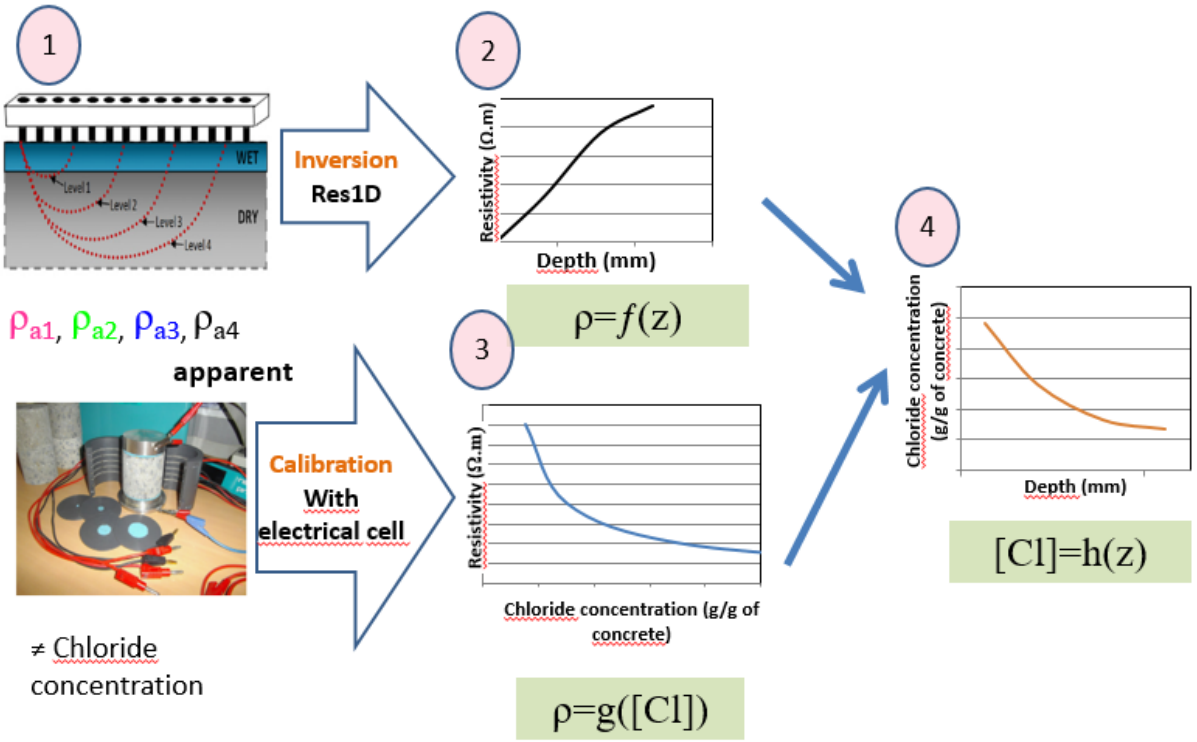

Figure 1 Schematic representation of the methodology used to obtain chloride content profiles in concrete

2.2 Resistivity measurement techniques

In this section, we present the two techniques, first, the resistivity cell for determining the calibration curves on cores and, second, the ERT device for carrying out apparent resistivity measurements in situ or on slabs at the lab scale. The resistivity cell as well the as the ERT device (also called resistivity probe in [18, 41]) used in this study were developed by Du Plooy et al. [41].

2.2.1 Electrical resistivity cell used for calibration

The main use of the resistivity cell is the measurement of the apparent resistivity of small concrete cores (75 mm diameter and 70 mm height) saturated with different chloride contents in order to establish the calibration curve specific to each material. The cell is made of a cylindrical PVC support in which five "ring" electrodes were placed (Figure 2 (a)). The electrodes are made of conductive metallic sponges that are carefully humidified before the test to insure a better contact with the concrete. An electrical current, of intensity *I*, is injected through two metallic plate electrodes placed on the top and bottom ends of the core respectively as shown in Figure 2 (a). Potential differences ΔV_i are then measured between the various ring pairs in order to assess the homogeneity of the core. The apparent resistivity ρ_{ai} for each ring pair is then obtained using (equation 1):

$$\rho_{ai} = G_i \frac{\Delta V_i}{I} \quad (1)$$

where G_i is a geometric factor equal to A/L_i (Figure 2) (where A is the area of each electrode plate and L_i the distance between the ring electrodes used). Four measurements are performed between two consecutive rings and two measurements are performed between the two extreme rings totalizing therefore six measurements.

In this study, having saturated the whole core in the same NaCl solution, we assume each core to be homogeneous. Therefore, regardless of the electrode configuration, all the ρ_{ai} theoretically equal the concrete resistivity. The measured apparent resistivities are averaged over all ring electrode pairs and the standard deviation is calculated and is considered as the uncertainty value of the measurements.

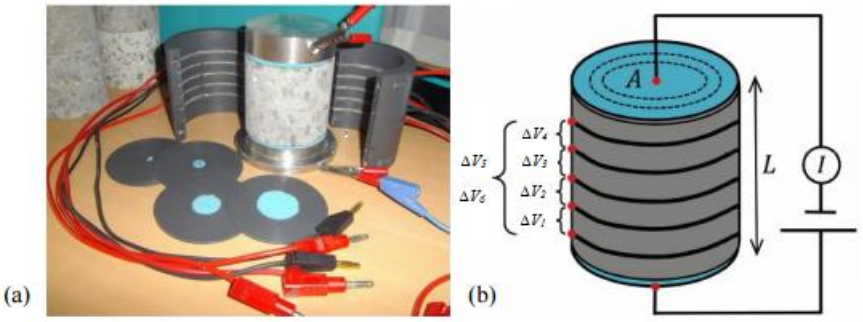

Figure 2 Electrical resistivity cell: the cell used (a) and schematic view of the general principle (b) [43]

2.2.2 Electrical Resistivity Tomography device

The ERT device (Figure 3) can be used in situ on concrete structures. In this study it was implemented on rectangular concrete slabs and used in Wenner configuration (Figure 3 (c)). This device was successfully used to image the penetration of water and different sodium chloride solutions in concrete slabs [40, 41, 43, 44] and was compared to other electromagnetic techniques and destructive methods. It is composed of 14 hollow metallic electrodes filled with wetted sponges. The distance between the centers of the electrodes is equal to 2 cm. The Wenner configuration was chosen due to its high signal-to-noise ratio and high sensitivity to resistivity variation with depth [42]. This electrode configuration implies that the electrodes are aligned and equally spaced and that the current is injected through two outer electrodes and the potential difference is measured between the two inner electrodes. By increasing the spacing between the electrodes, the investigation depth increases [43]. Having 14 electrodes, one has access to 4 different electrode spacings and therefore 4 different investigation depths referred to as “levels” as shown by Figure 3 (a).

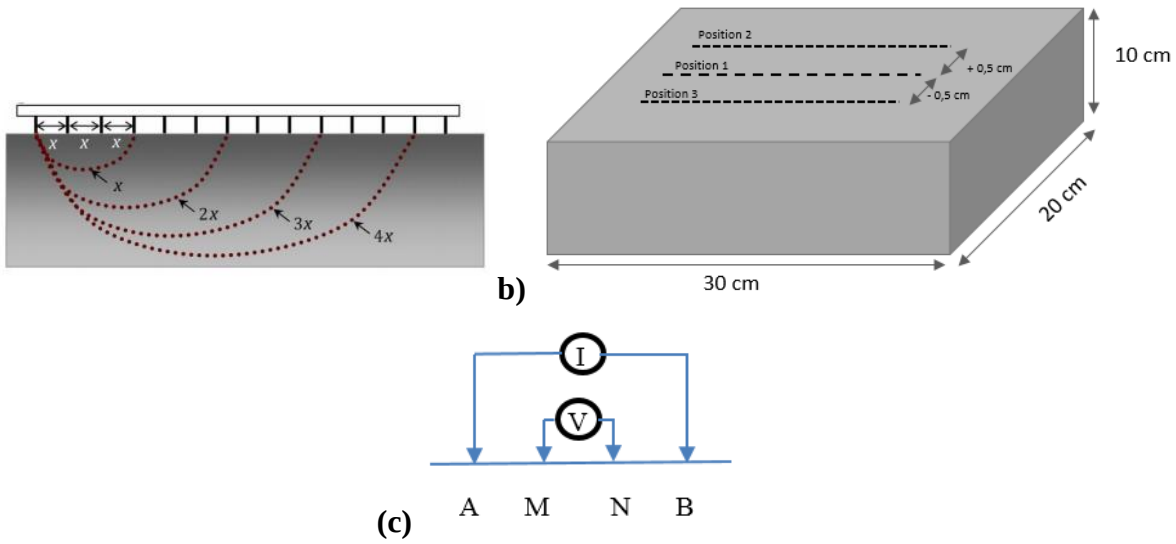

Figure 3 Schematic representation of the ERT device: (a) penetration depths, (b) device position on the slab, (c) Wenner configuration

Equation (1) is then applied to obtain the apparent resistivities with the geometric factors G. For an infinite homogeneous half-space medium, the geometric factor is equal to $G_R = 2\pi a$ where a is the spacing between the electrodes. However, for a finite medium, boundary conditions need to be taken into account. As explained in [41], the geometric factors in this study are calculated using the COMSOL Multiphysics finite element software and account for both the electrode spacing and the slab geometry.

It is worth noting that according to du Plooy [43] the modelled geometric factors are not influenced by the electrode sizes, whether they were modelled using point-electrodes or 4 mm diameter sponge electrodes.

As an example, the geometric factors obtained for the slab studied in the experimental program (section 3.3) are showed in Table 1.

As expected, the lowest geometric factors are found for the smallest electrode spacing and for the electrodes positioned near the edges. For more information on the analysis and determination of the geometric factors, the reader can refer to [41,43].

222

	Electrode spacing			
	a = 2 cm	a = 4 cm	a = 6 cm	a = 8 cm
G-Factors	0.1176			
	0.1216	0.202		
	0.1225	0.2106		
	0.1227	0.2129	0.2342	
	0.1228	0.2135	0.2408	0.2243
	0.1228	0.2135	0.2421	0.2243
	0.1228		0.2408	
	0.1227	0.2129	0.2342	
	0.1225	0.2106		
	0.1216	0.202		
	0.1176			

223 **Table 1: Geometric factors computed by FEM for the ERT deviced placed in the central upper face of a 30x20x10cm**
224 **slab**

225 As previously mentioned, for a non-homogeneous material, the obtained apparent resistivities
226 do not directly yield the 'true' resistivity distribution of the medium. To obtain the resistivity
227 distribution versus depth in the non-homogeneous, an inversion process is needed (step 2 in
228 our methodology). The inversion process is explained in section 2.3.

229 Three sets of measurements are performed: one in the middle of the slab (Position 1 in Figure
230 3 (b)) and two 5 mm apart from either side of the middle (Position 2 and 3 in Figure 3 (b)).
231 For each set of measurement: the number of electrode combinations and therefore the number
232 of apparent resistivity measured are 11 for Level 1 followed by 8 for Level 2, 5 for Level 3
233 and 2 for Level 4. The different values obtained for the three sets of measurement are
234 averaged per level and four apparent resistivity values are determined, one per investigation
235 level (ρ_{a1}, ρ_{a2}, ρ_{a3}, ρ_{a4}). The different values of apparent resistivity obtained per level can be
236 an indicator of the lateral heterogeneity of the slab. This factor is taken into account in this
237 study by the standard deviation of the different apparent resistivity values per level (σ_1, σ_2, σ_3,
238 σ_4). Since the volume investigated increases from Level 1 to Level 4, the effect of the vertical
239 heterogeneity on the measurement decreases when the electrode spacing increases.

240 **2.3 Inversion process of the measured apparent resistivities**

241 The inversion process consists in finding a resistivity profile (in 1D, or resistivity distribution
242 in 2D or 3D) that would yield the same measurements as the actual measurements on the
243 investigated medium [41, 45]. The inversion of the apparent resistivity values of the 4

different levels was carried out as stated before using Res1D which is a program based on Levenberg-Marquardt's algorithm (also known as damped least-squares [46]). Three sets of apparent resistivities were then chosen for the inversion: the mean values (ρ_{a1}, ρ_{a2}, ρ_{a3}, ρ_{a4}), the mean values plus the standard deviations (ρ_{a1} +σ_1, ρ_{a2} + σ_2, ρ_{a3}+ σ_3, ρ_{a4} + σ_4,) and the mean values minus the standard deviations (ρ_{a1} - σ_1, ρ_{a2} - σ_2, ρ_{a3} - σ_3, ρ_{a4} - σ_4). The reason for the three sets of inversion is to study the effect of the variability of the apparent measurements (data input) on the inverted resistivity profiles (data output).

The material was considered to be composed of 4 'homogeneous' layers (discrete parametrization) with predefined thicknesses estimated with Res1D using the electrodes configuration. The inverse problem consists in obtaining the resistivity values for each layer.

The resistivity profile was then estimated by displaying the resistivity at the center of each of the four layers (at 5.1, 16.57, 30.92 and 44.44 mm depth respectively) with horizontal lines corresponding to the thicknesses of the respective layers (equal to 10.2, 12.75, 15.94 and 20 mm).

It is worth noting that the thicknesses of the layers were determined by estimating the depth of investigation for each electrode separation [47]. This choice for the layer thicknesses may have an effect on the inverted results, i.e. the fitted resistivity of each layer and therefore the obtained resistivity profile. Indeed, it is a long established fact among the geophysics community that "electrical equivalences" may occur between layer models that yield the same apparent resistivities within the data uncertainty level (e.g. [48]). However, other inversion strategies not presented here (including not fixing the layer thicknesses and therefore inverting for both thicknesses and resistivities of layers) did not lead to better fits.

In future work, attention should be paid to the development of algorithms using optimized model parameterizations, e.g. a discrete parameterization based on a larger number of layers or a continuous parameterization based realistic resistivity profile shapes.

2.4 Destructive method to determine free chloride profiles

The adopted reference method is the well-known procedure recommended by the RILEM 178-TMC Technical Committee [12, 49]. In order to obtain a profile, the concrete specimens are ground in several steps of an average of 5-mm each, perpendicular to the top face of the specimen using a grinding instrument as recommended by Vennesland et al. [50]. This top face was in contact with the salted solution.

The procedure described below is used to determine the free chloride content from concrete powder [49, 51]. Approximately 5g of concrete powder is taken from each layer and placed in a beaker. To get free chloride, deionised water is added and the mixture is stirred for 3 min. The obtained solution is then filtered into a 250 cm^3 volumetric flask. The chloride concentration of the filtered solutions is determined by potentiometric titration with silver nitrate ($AgNO_3$).

It is worth noting that the total chloride content in concrete is the sum of the free chlorides in the pore solution and the chlorides that are bound to the cement paste (physically or chemically) [52]. In this research, we study mainly the free chlorides for two reasons: the first is that the corrosion risk of the steel mainly depends on the free chlorides and the second reason is that the electric current in concrete is carried by the ions present in the concrete pores solution [26].

3. Experimental program: materials, specimens and measurements procedures

The global methodology developed in section 2 was applied on an experimental program on 3 types of material. The descriptions of the experimental program as well as the measurement procedures are detailed in the following.

3.1 Concrete mix designs and specimens

The experimental program was carried out using 2 types of concrete: C1 and C2, and one type of mortar M2. The different components of the materials are represented in Table 2. Concrete C1 is an industrial concrete whereas the other materials were fabricated in the lab under controlled conditions. Concrete C1 was one year old at the time of the test and was kept under ambient temperature conditions in laboratory (T = 20±2°C and RH = 50±7%). C2 and M2 were around 8 years old at the time of the test and were conserved alternatively in water or ambient temperature. The three materials were chosen to have a water to cement ratio (W/C) superior to 0.6 to accelerate the penetration of aggressive agents.

	C1		C2 and M2		
Components (kg/m^3)	Origin	**C1 (kg/m^3)**	Origin	**C2 (kg/m^3)**	**M2 (kg/m^3)**
Aggregate (11/22)	Pont de Pierre, corneen	760		0	0
Aggregate (6/10)	Trégueux, amphibolite	320	Pontreaux, gneiss	785	0
Sand (0/4)	Moulin, alluvial	300	Pilier, alluvial	445	649
Sand (0/2)	Gouviard, gneiss	560	Pontreaux, gneiss	449	652
Cement C CEM I 52.5 N	Saint-Pierre la Cour, Lafarge	305	Saint-Pierre la Cour, Lafarge	341	492
Admixture, AD	Sika prise SC2	0.7		0	0
Added water				235	331.9
Effective water W		190		222.9	319.5
W/C	0.623			0.654	0.649
Percentage of cement paste (%)	0,3			0,36	0,51
Dmax [mm]	22			10	5

Table 2 Concrete mix design of concretes C1 and C2 and mortar M2

The concrete properties are given in Table 3: the values provided are the average values obtained from three experimental results. The open porosity was determined by water saturation under vacuum condition and the apparent diffusion coefficient was determined by chloride migration test in non-steady- state [53].

Material	Open porosity measured by water saturation at 90 days (%)	Apparent diffusion coefficient (x10-12 m2/s) [53]	Compressive strength at 28 days (MPa)
C1	15.9 ± 0.7	21.9 ± 7.6	36.3 ± 0.9
C2	17.5 ± 0.6	55.4	37.1 ± 0.8
M2	26.4 ± 0.5	62.1	34.0 ± 1.0

Table 3 Properties of concretes C1 and C2 and mortar M2

The experimental program included two main types of experiments: the calibration of the resistivity with respect to chloride content using concrete cores which will be presented in section 3.2, and the diffusion of chloride in saturated conditions using concrete slabs which will be presented in section 3.3.

Concerning the specimens, for each material, we dispose of 8 cores used for calibration (with a 75 mm diameter and a 70 mm height). Moreover, we dispose of four slabs (300x220x100 mm): two slabs for C1 (C1-1 and C1-2), one slab for C2 (C2-1) and one slab for M2 (M2-1) used for chloride diffusion.

3.2 Calibration: Core conditioning and measurement procedure with EM cell (Step 3 in Section 2.1)

For calibration purpose, the resistivity has to be measured at different chloride contents. For each 3 concretes, the 8 cores (∅75x70 mm) were initially dried in an oven at 65°C until mass stability according to the criteria defined by [54] (i.e. the relative difference of 2 weighing results with a 24h gap must be under 0.05%). We assume actually that the studied concrete materials are fully hydrated and hydrates like ettringite remain stable below 70°C [55]. The 8 cores were afterwards saturated using a vacuum-chamber with solutions having 4 different sodium chloride concentrations (0, 15, 35 and 90 g/L) in addition to 4 g/L NaOH to avoid leaching as recommended by the French standards [56-57] (2 cores per concentration). The cores were then stored for 5 months in a solution (regularly renewed) with the same sodium chloride concentration as the one they were saturated with.

For each concentration, two cores of each concrete were conditioned and tested with the resistivity cell in order to obtain the calibration curves. After the first set of 6 measurements is performed, the core is rotated and a second set of 6 measurements is performed. Having 12 resistivity measurements per core (at different heights of the core), the total number of resistivity measurements is 24 per material per concentration. The average of the 24 measurements as well as the standard-deviation are computed.

At the end of the non-destructive testing, the “real” free chloride concentrations were determined for one of the two cores at 4 different heights (approximately 5, 20, 40 and 60 mm), using the destructive protocol detailed in section 2.4. To get the concentration at 5 mm, the core was ground in several steps from 0 to 10 mm, perpendicular to the top face of the specimen using the grinding instrument. To get the value at 20 mm, 40 mm and 60 mm, the core was ground respectively from 10 to 30 mm, from 30 to 50 mm, and from 50 to 70 mm.

The average of the concentrations obtained at the four different heights as well as the standard deviation were then calculated and are presented in the calibration curves (Figure 5) in section 4.1.

3.3 Chloride diffusion monitoring: Slab conditioning and non-destructive testing procedure with ERT device

The chloride diffusion experimental program was carried out under saturated conditions which entails that the main mode of transport of chloride ions is due to the concentration difference between the external solution and the interstitial water. In preparation for the diffusion experimental program, the 4 slabs (C1-1 and C1-2, C2-1, M2-1) were saturated in a vacuum chamber with chloride free tap water. An epoxy resin was then applied on the lateral faces of the slab to ensure a unidirectional transfer.

The slabs were then placed in individual closed boxes. The bottom face was placed in regularly renewed solutions containing 165 g/l NaCl and 4 g/l NaOH up to 1 cm, at initial test time. The upper face was covered with a wet cloth to prevent evaporation (see Figure 4).

At each test time, each slab was removed from solution and carefully wiped with a wet cloth before apparent resistivity measurement with the ERT device. The measurements were carried out at the 3 positions indicated at section 2.2.2 and on both sides. Right after the measurements, the slab was placed again in the solution again in the same way as for the initial test time.

Using this same protocol, the apparent resistivity measurements were regularly performed for a period of 18 weeks for C1-1, 40 weeks for C1-2 and 12 weeks for each of C2-1 and M2-1.

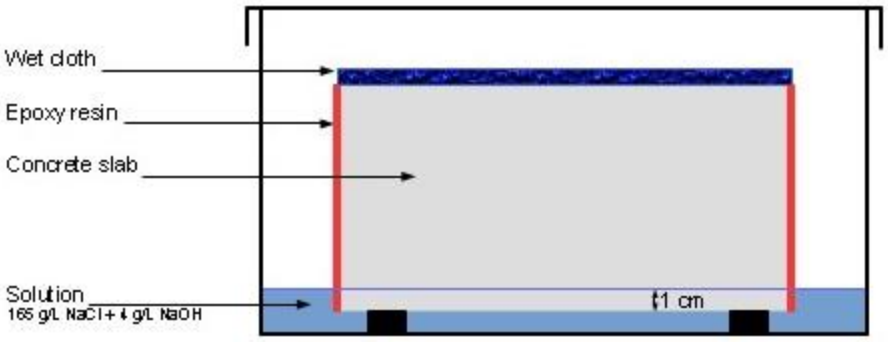

Figure 4 Scheme of the chloride diffusion protocol

4. Results and discussions

In this section, the calibration curves and the monitoring (in terms of apparent resistivity and true resistivity profiles) of the chloride diffusion in saturated slabs are presented. Then an

370 analysis of uncertainty sources is led. Finally, the chloride content profiles extracted from
371 ERT measurements are compared to reference destructive profiles at final test times.

372

373 **4.1 Calibration results: Chloride concentration as a function of resistivity (Step 3)**
374 As explained before, the calibration curves are needed to convert the resistivity profile
375 obtained in step 2 into chloride concentration profile (step 4). It is shown in this paragraph
376 how the calibration curves are obtained for each concrete.

377 The resistivity versus chloride concentration calibration curves for the three materials are
378 presented in Figure 5. The average resistivity (standard-deviation given by vertical error bars)
379 measured in homogeneous cores is function of the average of the concentrations (standard
380 deviation as horizontal error bars) obtained by the reference chloride titration. For all the
381 cases, the chloride content was found to be homogeneous throughout the core with the
382 maximal variation coefficient attaining 6%.

383 In order to compare the materials, in Figure 5 (a) we represent the concretes C1 and C2, and
384 in Figure 5 (b) we represent the concrete C2 and mortar M2. The experimental results show a
385 fast decrease of the resistivity at low concentrations and a slow decrease at higher
386 concentrations, similarly to the results of [31], [32] and [58]. Therefore, the results were
387 modeled using an exponential curve with regression coefficients superior to 0.9. Three curves
388 were obtained by fitting the average experimental points (blue solid line) and the average plus
389 and minus the vertical and horizontal standard-deviation (pink and green dashed lines).

390 As mentioned before, the resistivity and the diffusivity of concrete are strongly related since
391 they are both dependent on the tortuosity and porosity of the material. When the diffusivity is
392 higher, the current is lead more easily through the concrete and the resistivity is therefore
393 lower. Comparing the two concretes, the resistivity of the saturated concrete C1 (initially
394 around 50 Ω.m) is superior to that of the saturated C2 (initially around 30 Ω.m), the latter
395 being superior to that of M2 (initially around 20 Ω.m). The results are in agreement with the
396 values obtained for the apparent coefficient of diffusion (Table 3) where that of C1 (21.7×10^{-12}
397 m^2/s) is inferior to that of C2 (55.4×10^{-12} m^2/s), the latter being inferior to that of M2
398 (62.1×10^{-12} m^2/s). This general trend also applies for the samples with chloride.

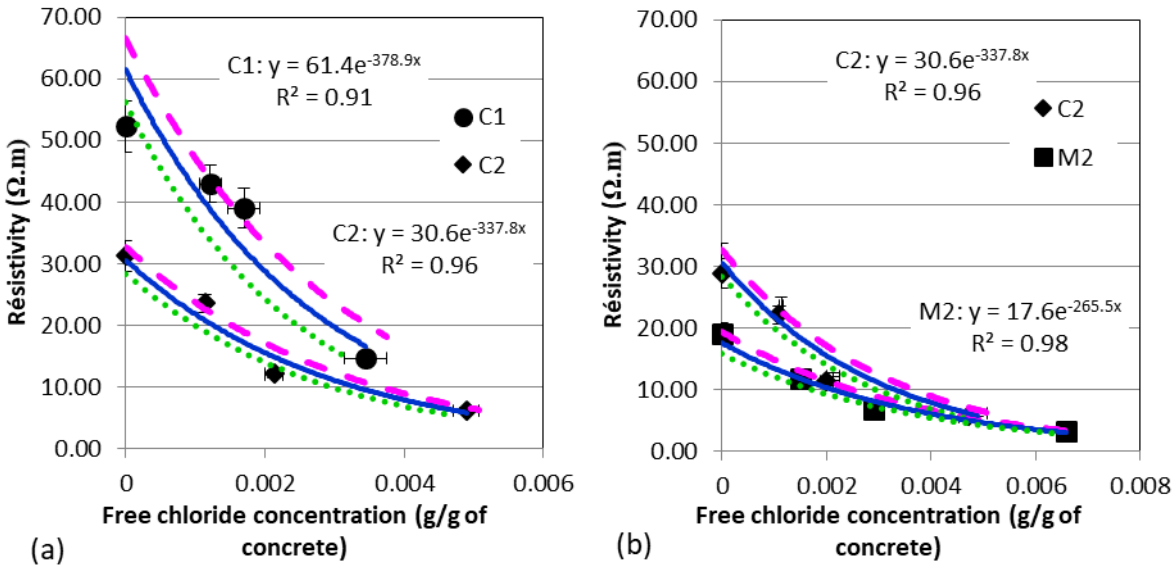

Figure 5 Calibration curves relating resistivity versus free chloride concentrations - (a) concretes C1 and C2 - (b) concrete C2 and mortar M2

4.2 Monitoring resistivity versus time during chloride diffusion process (Step 1)

We present herein the chloride diffusion monitoring results. The apparent resistivities of the concretes measured during the experimental program are inverted. Then the true resistivity profiles are translated into chloride concentrations using the calibration curves.

4.2.2 Variation of resistivity with time during chloride diffusion

4.2.2.1 Initial state

The apparent resistivity measured for each Level (Level 1 to 4) versus time of diffusion is presented in Figure .

As indicated before, the slabs were saturated in vacuum in order to obtain a homogeneous saturated slab (saturation = 100%, chloride concentration = 0 g/l). Therefore, at the initial state, the resistivity results at the different levels (or different investigated depths) were expected to be equal. However, the apparent resistivity at Level 1 is superior to the resistivity of the other Levels indicating an initial property gradient in the concrete (Table 4). This initial gradient can either be due to a porosity difference (due to carbonation, framework effects, shrinkage, …) or to an ionic difference in the material (leaching).

The carbonation hypothesis was dismissed considering that prior to the experiment, the slabs were cut (about 1 cm) from all sides in order to remove any carbonated portion of the concrete. Considering that the specimens were stored in tap water, the resistivity gradient was

valued to be more likely due to a possible leaching whose influence on resistivity measurement is underlined by [20] and not to carbonation or water saturation degree difference. In the future, we plan to control the basicity of the solution in which the concrete is stored in order to avoid any risk of lixiviation problem. In addition, compared to the initial state of the cores used for calibration (Table 4), the resistivity values of the slabs of C1 were expected to be higher, and those of the slabs of C2 and M2 were expected to be lower. The difference between the resistivity values almost certainly lies in the material heterogeneity. This difficulty will be a challenge for in-situ measurements given that the contrast between the samples will be even higher than in the case of laboratory conditions.

	Apparent resistivity at the initial state (Ωm) Saturation degree = 100 %, Chloride concentration = 0						
	Slab				Material (Average values of 2 cores)		
Levels	C1-1	C1-2	C2-1	M2-1	C1	C2	M2
Level 1	43.61	46.92	37.95	27.03	52.7	31.26	19.19
Level 2	38.22	38.73	34.79	24.37			
Level 3	36.63	37.50	33.93	24.28			
Level 4	37.54	37.65	33.66	24.51			

Table 4 Initial state of the slabs : apparent resisitivty values for Levels 1 to 4

4.2.2.2 Evolution of apparent resistivity with time

For the 4 slabs, the trend of the curves are similar: a decrease of the apparent resistivity values for the 4 levels is noticed due to the penetration of chloride in the concrete. For concrete C1, we chose to prolong the diffusion test for the slab C1-2 up to 40 weeks compared to 18 weeks of test time in the case of slab C1-1. The apparent resistivity values of the four levels continue to mildly decrease after 18 weeks. The standard-deviation (of the three series of measurements) is the highest for Level 1 and decreases from Level 1 to Level 4. Given that the measurement for each Level integrates a certain volume of the slab which increases from Level 1 to Level 4, the resistivity values at Level 4 are less influenced by the local variation in the material.

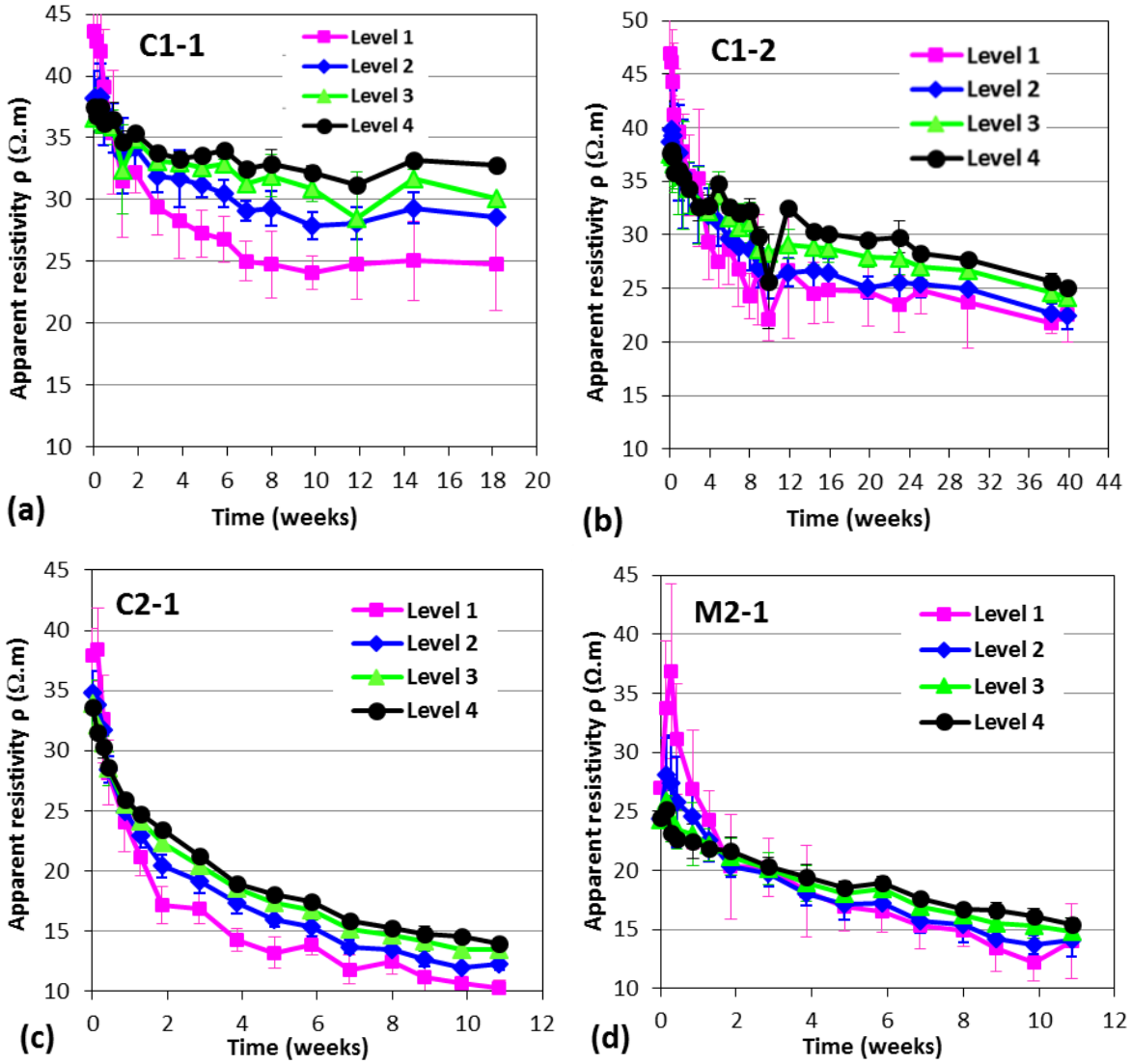

Figure 6 Evolution of apparent resistivity versus time during a chloride diffusion test for Level 1 to 4 for: slab C1-1 (a), C1-2 (b), C2-1 (c) and mortar M2-1 (d)

Within few days of exposure to chloride , the apparent resistivity values for a given date is increasing from Level 1 to Level 4 which implies a lower resistivity on the surface and a higher resistivity in the core. This is in agreement with the expected direction of chloride ions: from the surface to the core. Therefore, the results indicate a high chloride concentration on the surface and a lower concentration in the core which is in agreement with the physical law of chloride diffusion.

The raw results displayed offer a good indicator of the chlorides penetration in the concrete without destroying the samples and can be used as such on-site to monitor the evolution of the state of the material. Therefore, by simply performing surface resistivity measurements on the

structure, the apparent resistivity can indicate an increase or a decrease of the chloride concentration for a stable saturation degree.

However, for a higher accuracy, it would be very useful to obtain not merely the trend of the concentration, but the exact distribution of the chloride concentration in concrete. The next section deals with the sources of uncertainty encountered in the process of obtaining the chloride concentration profile.

4.3 Apparent resistivity inversion and sources of uncertainty on the chloride profiles (Step 2 and 4)

As detailed in section 2.1, different steps are required to obtain chloride profile from surface resistivity measurements. The steps include mainly an inversion and a calibration process. The variability of the raw data, the material difference between the calibration cores and the diffusion slabs are all sources of uncertainty that will affect the final results. Taking them into account is crucially important and in the next section, a first attempt is presented.

The study of the propagation of the uncertainty throughout the different steps of the method is presented solely for concrete C2 as an example. The same analysis was applied to C1 and M2, and the final result will be presented for the 3 materials.

4.3.1 Consequences of raw data variability on the inversion results

As was elaborated in section 3.3, three sets of raw data were chosen for inversion taking into account the standard deviation. So, the resistivity ρ correspond to the inversion result of the average apparent resistivity ρ_a and the resistivities, noted ρ- and ρ+ , correspond respectively to the inversion results of $\rho_a - \sigma$ and $\rho_a + \sigma$. As an example, the three sets of inversion after 0.9 week, 3 weeks, and 11 weeks of concrete C2 are displayed in Figure 7 (a). Three resistivity profiles for each date are obtained: a mean profile ρ (solid line), a maximal profile ρ+ (dotted lines) and a minimal profile ρ- (dashed lines). We remind the reader that the inversion was carried out using a discrete parameterization and horizontal error bars represent the layers thickness. The horizontal bars are represented solely for the inversion of the mean resistivity after 3 weeks of chloride diffusion for visual purposes.

To visualize the effect of the resistivity profiles variability on chloride profiles, in Figure 7 (b) we display the three sets of chloride profiles at 11 weeks of diffusion obtained using the three sets of resistivity profiles and the mean curve of calibration (Figure 5 (b)). However, the

487 calibration curves present as well a maximal and minimal variation range that needs to be
488 taken into account.

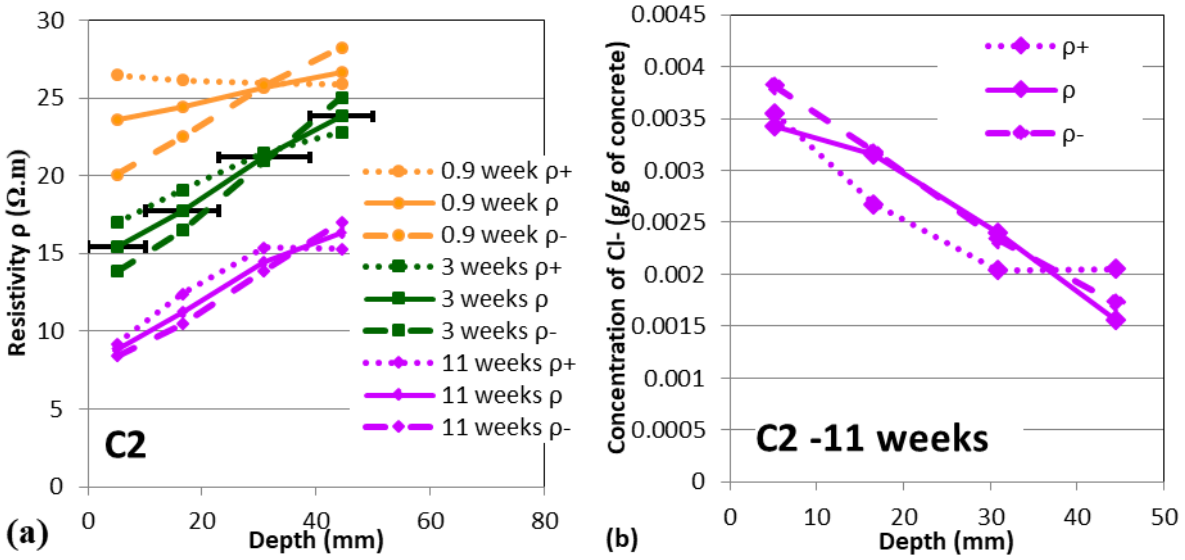

489

490 **Figure 7 Consequences of raw data variability for concrete C2 on the profiles: (a) resistivity profile after 0.9 week, 3**
491 **and 11 weeks (b) chloride profile after 11 weeks**

492

493 **4.3.2 Consequences of calibration curve variability on the inversion results**

494 The mean resistivity profile obtained after 11 weeks of diffusion (purple solid line in Figure 7
495 (a)) is converted to three chloride profiles (Figure 8 (a) maximal in pink, mean in blue and
496 minimal in green) using the three calibration curves (Figure 5 (b)). The same procedure was
497 applied for the minimal resistivity profile « ρ- » (Figure 8 (b)) and maximal resistivity profile
498 « ρ+ » (Figure 8(c)). Finally, 9 profiles are obtained. In order to assess and show the range of
499 uncertainty, three of the 9 chloride profiles were selected (Figure 9 (c)): the mean profile
500 (solid blue line), the maximal profile (pink dashed line, noted Cl max ρ-) and the minimal
501 profile (dotted green line, noted Cl min ρ+). The drawback is that this choice maximizes the
502 possible variation range of the uncertainty.

503 For the two other materials, the same procedure was applied thus the mean resistivity profile ρ
504 is shown and the variation range between "Cl max ρ-" and "Cl min ρ+".

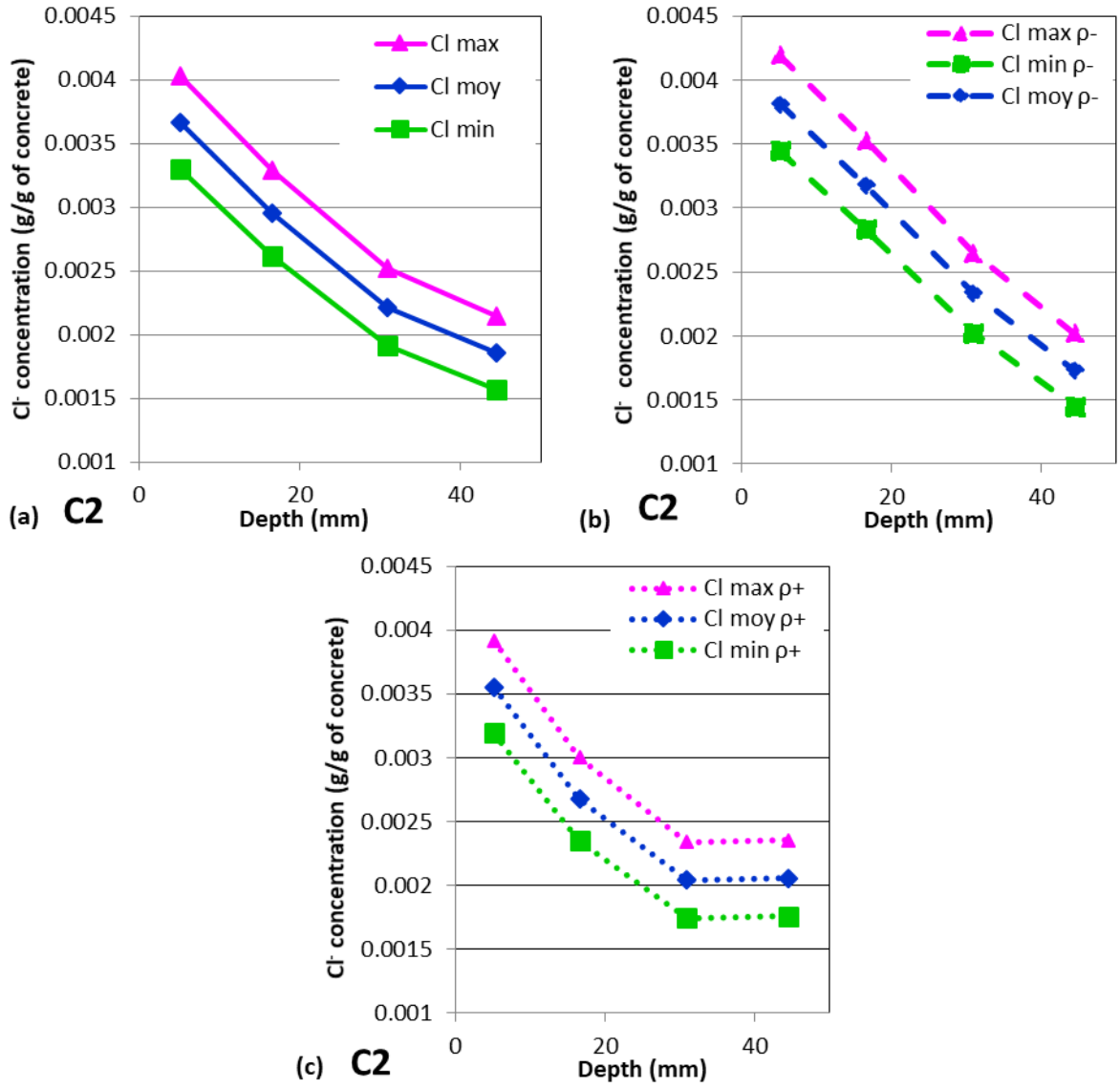

Figure 8 Concrete C2 after 11 weeks of diffusion: Minimal, mean, maximal profiles for the inversions of ρ (a), ρ- (b) et ρ+ (c)

4.4 Comparing chloride profiles obtained by resistivity to those obtained by destructive method

The procedure explained in the previous sections has been applied to the three materials: C1, C2 and M2. In addition, for each slab, a destructive chloride profile was obtained using a core (70 cm diameter) from the slab. In Figure 9, the chloride profiles obtained by resistivity are illustrated in three colors (green, blue and pink) and the one obtained by potentiometric titration in black. The vertical error bars for the destructive methods are based on a recent study by Bonnet et. al [59] where the vertical standard deviation for total chloride content is approximately equal to 6% (calculated from 42 measurements). Unfortunately, no studies are found about the sources of uncertainties for the free chloride profile measurements in concrete

by destructive method. However, as explained in [59], the protocol for obtaining the total and free chloride profiles are similar.

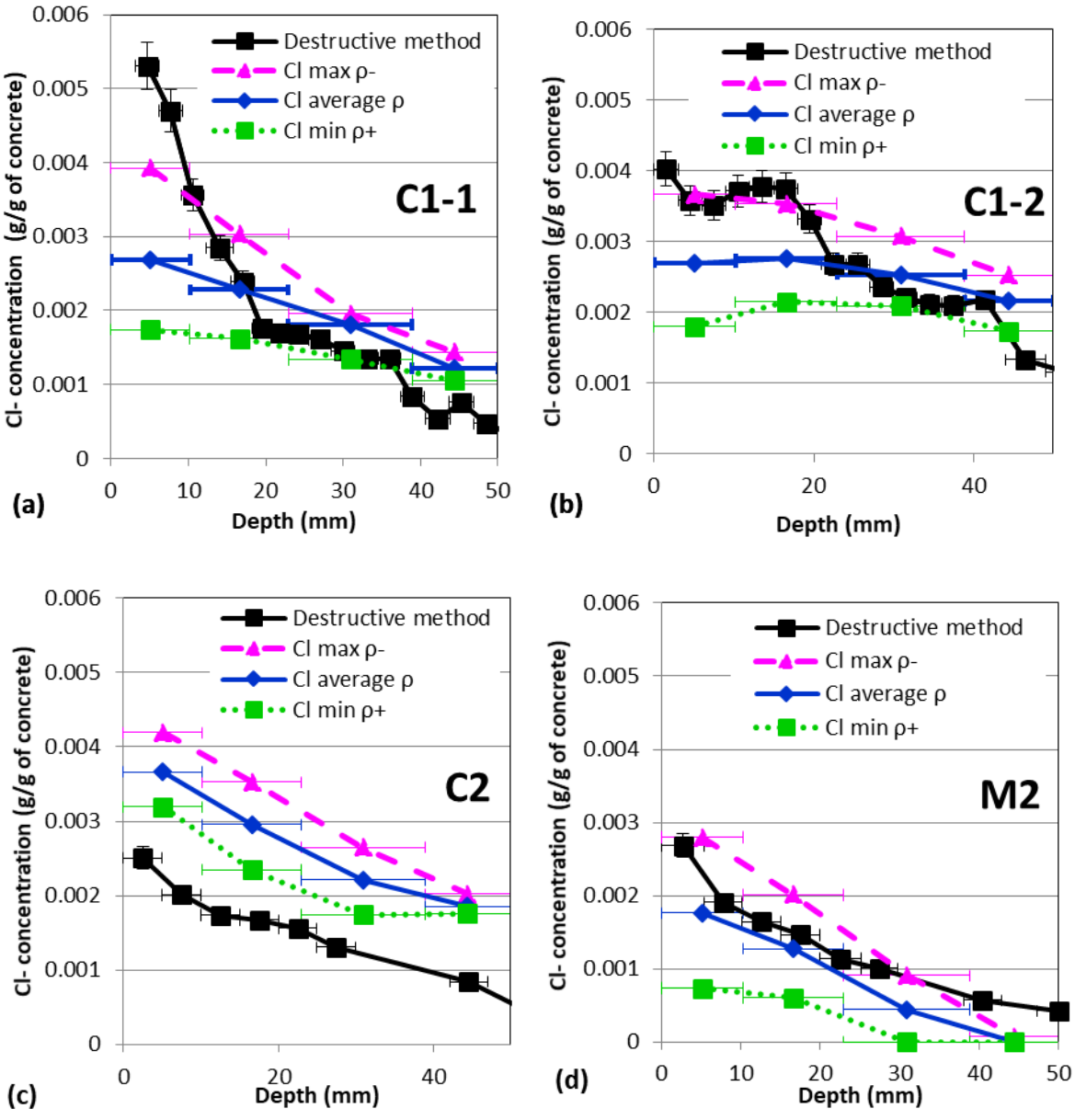

Figure 9 Comparing chloride profiles obtained by resistivity and those obtained by destructive method for : Slabs C1-1 (a), C1-2 (b), C2 -1 (c) and M2-1 (d)

In general, and considering the horizontal error bars, the destructive profiles lie in the range of the non-destructive profiles. The few differences that can be found between the profiles are attributed to the several sources of uncertainty stated before. More specifically, two main sources can be underlined:

1) The inversion process yields four resistivity values at four layers represented by the horizontal error bars. The thickness of the layers is quite important and makes it difficult to deduce a profile.

2) At the initial state (concrete fully saturated and without chloride), a significant difference was found between the resistivity of the slabs used for the diffusion test and the cores used for the calibration (Table 4). Since the curves displayed in Figure 9 were obtained using those calibration curves, a significant difference between the ND results and the D results is expected.

The diffusion of chloride for concrete C1 lasted for 18 weeks for slab C1-1 (solid line in Figure 10) and for 40 weeks for slab C1-2 (dashed lines in Figure 10). The comparison of the chloride profiles obtained by means of both resistivity and destructive method at the end of the experimental program is presented in Figure 10.

The increase of the chloride concentration from 18 weeks (C1-1) to 40 weeks (C1-2) is observed for both the ND and the D profiles. In addition, between the depths of 20 and 36 mm, the ND and the D profiles are almost merged.

The D profile of C1-1 is superior to that of C1-2 between the depths of 0 and 10.6 mm. This is certainly due to the material difference between both slabs. As stated earlier, the material heterogeneity effect is more pronounced on the surface of the slabs.

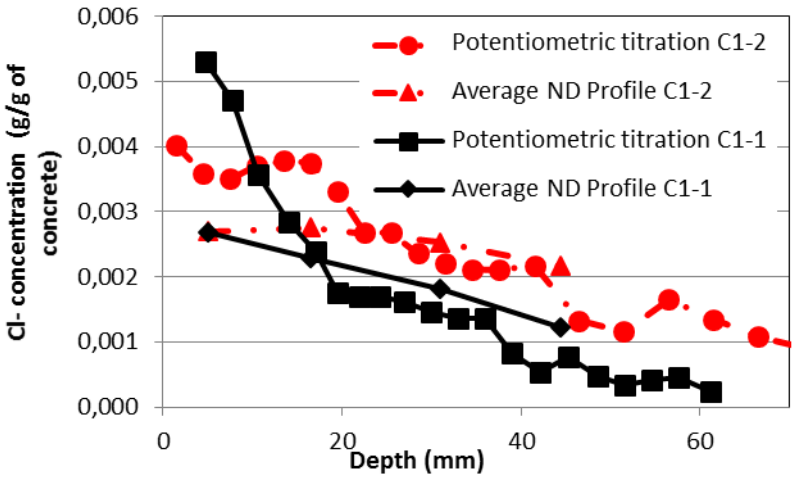

Figure 10 Evolution of chloride profiles for concrete C1 after 18 weeks (slab C1-1) and 40 weeks of chloride diffusion (slab C1-2)

5 Conclusion

In this article, we have presented a methodology that allows obtaining chloride concentration profiles from surface resistivity measurements. The process implies the use of an inversion process to obtain resistivity profiles and a calibration curve to obtain chloride concentration

profiles. The methodology was successfully applied to three types of material (two concretes and one mortar). The profiles obtained were compared to those obtained by a destructive method. The non-destructive results were represented by three profiles for each measurement: a mean/intermediate, a maximal and a minimal profile. The three profiles took into consideration the propagation of uncertainty throughout the proposed methodology. In general, the destructive profile was located between the gaps of the three profiles. The highest sources of uncertainty underlined were first the material difference between the samples used for calibration (cores) and those used for the diffusion tests (slabs), and second the automatic inversion process that only allows a discrete parametrization of the modelled medium.

To overcome the uncertainty from the inversion process, several solutions can be studied such as the implementation of a continuous parametrization inversion and/or the increase of the number of available data. However, overcoming the uncertainty coming from the material differences is trickier because as stated before, the material difference at on-site measurements is more important than that of laboratory samples. In this case, increasing information about the material (by increasing and varying non-destructive techniques) can aim to assess the difference between the measured samples and those used for calibration. Therefore, the difference can be implemented in the calibration curves and taken in consideration when transforming resistivity values to chloride concentrations.

The comparison of two chloride concentration profiles for the same concrete after two different diffusion times highlights the ability of the methodology to monitor the evolution of chloride penetration. In the near future, the study of the evolution of the chloride concentration profiles by means of resistivity can aim to determine durability indicators using chloride penetration models.

Acknowledgments

The authors would like to thank Région Pays de la Loire and IFSTTAR for financial support of the PhD thesis, IFSTTAR and CEREMA for financing the research project ORSI-APOS, Véronique Bouteiller and Jean-Luc Geffard (IFSTTAR), Ronan Queguiner and the technical team from CEREMA Site of Saint Brieuc, for their contribution in the experimental campaign.

Bibliography

[1] V. Baroghel-Bouny, Concrete design for structures with predefined service life durability control with respect to reinforcement corrosion and alkali–silica reaction state-of-the-art and guide for the implementation of a performance-type and predictive approach based upon durability indicators, English version of Documents Scientifiques et Techniques de l'AFGC (Civil Engineering French Association) (2004) 252.

[2] L. Pang, Q. Li, Service life prediction of RC structures in marine environment using long term chloride ingress data: Comparison between exposure trials and real structure surveys, Construction and Building Materials 113 (2016) 979–987.

[3] W. Chalee, C. Jaturapitakkul, P. Chindaprasirt, Predicting the chloride penetration of fly ash concrete in seawater, Marine Structures 22 (2009) 341–353.

[4] I. Othmen, S. Bonnet, F. Schoefs, Investigation of different analysis methods for chloride profiles within a real structure in a marine environment, Ocean Engineering, Volume 157, pp 96-107.

[5] Hilsdorf, H., Kropp, J., 2004. Performance Criteria for Concrete Durability, CRC Press, 2004.

[6] A.B. Fraj, S. Bonnet, A. Khelidj, New approach for coupled chloride/moisture transport in non-saturated concrete with and without slag, Construction and Building Materials 35 (2012) 761-771.

[7] A. Da Costa, M. Fenaux, J. Fernández, E. Sánchez, A. Moragues, Modelling of chloride penetration into non-saturated concrete: Case study application for real marine offshore structures, Construction and Building Materials 43 (2013) 217–224.

[8] L. Bertolini, B. Elsener, P. Pedeferri, E. Redaelli, R. Polder, Corrosion of steel in concrete: Prevention, Diagnosis, Repair, 2nd Edition, WILEY-VCH, Weinheim, Germany, 2013.

[9] A. Neville, Chloride attack of reinforced concrete: an overview, Materials and Structures 28 (1995) 63-70.

[10] K. Tuutti, Corrosion of Steel in Concrete, Swedish foundation for concrete Research, Stockholm, 1982.

618 [11] U. Angst, B. Elsener, C.K. Larsen, & Ø. Vennesland, Critical chloride content in
619 reinforced concrete—a review. Cement and concrete research 39(12) (2009) 1122-1138.

620 [12] R.T. 178-TMC, Analysis of total chloride content in conrete, Materials and Structures 35
621 (2002 (a)) 583-585.

622 [13] D. Breysse ed., Non-destructive Assessment of Concrete Structures: Reliability and
623 Limits of Single and Combined Techniques: State-of-the-art Report of the RILEM Technical
624 Committee 207-INR, Springer, Netherlands, 2012.

625 [14] J.G. Webster, H. Eren, Measurement, Instrumentation, and Sensors Handbook, Second
626 Edition:Spatial, Mechanical, Thermal, and Radiation Measurement., CRC Press,2014.

627 [15] G.E. Monfore, The electrical resistivity of concrete., Journal of PCA (1968) 35-48.

628 [16] A. Robert, Dielectric permittivity of concrete between 50 Mhz and 1 Ghz and GPR
629 measurements for building materials evaluation, Journal of Applied Geophysics 40(1-3)
630 (1998) 89-94.

631 [17] D.A. Whiting, M.A. Nagi, Electrical resistivity of concrete – a literature review, Portland
632 Cemente Association, Skokie (Illinois),2003.

633 [18] R. du Plooy, G. Villain, S. Palma Lopes, A. Ihamouten, X. Dérobert, B. Thauvin,
634 Electromagnetic non-destructive evaluation techniques for the monitoring of water and
635 chloride ingress into concrete: a comparative study, Materials and structures 48 (2015) 369-
636 386.

637 [19] R.B. Polder, W.H.A. Peelen, Characterisation of chloride transport and reinforcement
638 corrosion in concrete under cyclic wetting and drying by electrical resistivity, Cement and
639 Concrete Composites 24(5) (Octobre 2002) 427-435.

640 [20] R. Spragg, S. Jones, Y. Bu, Y. Lu, D. Bentz, K. Snyder, J. Weiss, Leaching of
641 conductive species: Implications to measurements of electrical resistivity., Cement and
642 Concrete Composites 79 (May 2017) 94-105.

643 [21] Y. Bu, J. Weiss, The influence of alkali content on the electrical resistivity and transport
644 properties of cementitious materials., Cement and Concrete Composites 51 (August 2014) 49-
645 58.

[22] M. Fares, Y. Fargier, G. Villain, X. Dérobert, S. Palma Lopes, Determining the permittivity profile inside reinforced concrete using capacitive probes, NDT&E international 79 (2016) 150-161.

[23] G. Klysz, J.P. Balayssac, Determination of volumetric water content of concrete using ground-penetrating radar, Cement and concrete research 37(8) (2007) 1164-1171.

[24] X. Dérobert, J. Iaquinta, G. Klysz, J.P. Balayssac, Use of capacitive and GPR techniques for non-destructive evaluation of cover concrete, NDT&E International. 41(1) (2008) 44-52.

[25] G. Villain, V. Garnier, M. Sbartaï, X. Dérobert, J-P. Balayssac, Development of a calibration methodology to improve the on-site non-destructive evaluation of concrete durability indicators, Materials and Structures, 2018, 51:40 available on line https://doi.org/10.1617/s11527-018-1165-4

[26] R.B. Polder, Test methods for on site measurement of resistivity of concrete -- a RILEM TC-154 technical recommendation, Construction and Building Materials 15(2-3) (2001) 125-131.

[27] C. Andrade, A. R., Concrete mixture design based on electrical resistivity, Second International Conference on Sustainable Construction Materials and Technologies, Ancona, Italy, 2010, pp. 28-30.

[28] H.W. Whittington, J. McCarter, M.C. Forde, The conduction of electricity through concrete, Magazine of Concrete Research 33(114) (1981) 48-60.

[29] B.P. Hughes, A.K.O. Soleit , R.W. Brierley New technique for determining the electrical resistivity of concrete, Magazine of Concrete Research 37(133) (1985) 243 –248.

[30] W. Elkey, E.J. Sellevold, S. Vegvesen, Electrical resistivity of concrete, Publication No. 80 (1995).

[31] M. Saleem, M. Shameem, S.E. Hussain, M. Maslehuddin, Effect of moisture, chloride and sulphate contamination on the electrical resistivity of Portland cement concrete, Construction and Building Materials 10 (3) (1996) 209-214.

[32] Z.M. Sbartaï, S. Laurens, J. Rhazi, J.P. Balayssac, G. Arliguie, Using radar direct wave for concrete condition assessment: Correlation with electrical resistivity., Journal of Applied Geophysics 62(4) (2007) 361-374.

675 [33] J.F. Lataste, G. Villain, J.P. Balayssac. Chapter 4. Electrical Methods, IN Non-
676 destructive Testing and Evaluation of Civil Engineering Structures, BALAYSSAC J-P.,
677 GARNIER V. (Eds). Elsevier Press Ltd, Amsterdam, English Version (2017) 356p. ISBN
678 978-1-78548-229-8 https://doi.org/10.1016/B978-1-78548-229-8.50004-2

679 [34] S. Bonnet, J.P. Balayssac, Combination of the Wenner resistivimeter and Torrent
680 Permeameter methods for assessing carbonation depth and saturation level of concrete,
681 Construction and Building Materials, 188 (2018), pp. 1149-1165.

682 [35] A. Lübeck, A.L.G. Gastaldini, D.S. Barin, H.C. Siqueira, Compressive strength and
683 electrical properties of concrete with white Portland cement and blast-furnace slag, Cement
684 and Concrete Composites 34(3) (2012) 392–399.

685 [36] W.J. McCarter, T.M. Chrisp, A. Butler, P.A.M. Basheer, Near surface sensors for
686 condition monitoring of cover-zone concrete, Construction and Building Materials15(2-3)
687 (2001) 115-124.

688 [37] R. Bässler, J. Mietz, M. Raupach, O. Klinghoffer, Corrosion monitoring sensors
689 fordurability assessment of reinforced concrete structures, Materials week, Munich, Germany,
690 September 25th-28th, 2000

691 [38] O. Banton, M.A. Cimon, M.K. Seguin, Mapping field-scale physical properties of soil
692 with electrical resistivity, Soil Science Society of America Journal 61(4) (1997) 1010-10.

693 [39] M.H. Loke, J.E. Chambers, D.F. Rucker, O. Kuras, P.B. Wilkinson, Recent
694 developments in the direct-current geoelectrical imaging method, Journal of Applied
695 Geophysics 95 (2013) 135–156.

696 [40] Y. Lecieux, F. Schoefs, S. Bonnet, T. Lecieux, S.P. Lopes, Quantification and
697 uncertainty analysis of a structural monitoring device: detection of chloride in concrete using
698 DC electrical resistivity measurement, Nondestructive Testing and Evaluation 30(3) (2015)
699 216-232.

700 [41] R. du Plooy, S. Palma Lopes, G. Villain, X. Dérobert, Development of a multi-ring
701 resistivity cell and multi-electrode resistivity probe for investigation of cover concrete
702 condition, NDT & E International 54(27-36) (2013).

703 [42] M.H. Loke, Electrical Imaging Surveys for Environmental and Engineering Studies: A
704 Practical Guide to 2-D and 3-D Surveys, (1999).

[43] R. du Plooy, The development and combination of electromagnetic non-destructive evaluation techniques for the assessment of cover concrete condition prior to corrosion, PhD-Université de Nantes, Ifsttar Nantes, 2013.

[44] G. Villain, A. Ihamouten, R. du Plooy, S. Palma Lopes, X. Dérobert, Use of electromagnetic non-destructive techniques for monitoring water and chloride ingress into concrete, Near Surface Geophysics 13(3) (2015) 299-309.

[45] W. Menke, Geophysical Data Analysis: Discrete Inverse Theory, Academic press 1989.

[46] M. Fares, Evaluation de gradients de teneur en eau et en chlorures par méthodes électromagnétiques non-destructives, PhD, Ecole Centrale de Nantes, Ifsttar, Nantes, 2015.

[47] R.D. Barker, Depth of investigation of collinear symmetrical four-electrode arrays. Geophysics 54(8) (1989) 1031-1037.

[48] D.S. Parasnis, Principles of applied geophysics. Fourth edition, Chapman & Hall (1986) 422 p.

[49] R.T. 178-TMC, Analysis of water soluble chloride content in concrete, Recommendation, Materials and Structures 35 (2002 (b)) 586-588.

[50] O. Vennesland, M.-A. Climent, C. Andrade, Recommendation of RILEM TC 178-TMC : Testing and modelling chloride penetration in concrete. Methods for obtaining dust samples by means of grinding concrete in order to determine the chloride concentration profile, Mater Struct : RILEM Technical Committee (2012).

[51] T. Chaussadent, G. Arliguie, AFREM test procedures concerning chlorides in concrete: extraction and titration methods, Materials and structures 32(3) (1999) 230-234.

[52] V. Baroghel-Bouny, X. Wang, M. Thiery, M. Saillio, F. Barberon, Prediction of chloride binding isotherms of cementitious materials by analytical model or numerical inverse analysis, Cement and Concrete Research 42(9) (2012) 1207-1224.

[53] N.B. 492, Nordest Method : Chloride migration coefficient from non-steady-state migration experiments, NORDTEST, Espoo, Finland (1999).

[54] AFPC-AFREM, Méthodes recommandées pour la mesure des grandeurs associées à la durabilité, Journées techniques AFPC-AFREM sur la durabilité des bétons, Toulouse–France, 1997, 283p.

[55] Zhou, Q., Glasser, F. P.,Thermal Stability and Decomposition Mechanisms of Ettringite at <120°C. Cement and Concrete Research, 2001, Vol. 31(9), pp.1333-1339.

[56] XP P 18-461, Concrete — Chloride migration of hardened concrete in steady state, French standards, AFNOR (2012).

[57] XP P 18-462, Concrete — Chloride migration of hardened concrete in non steady state, French standards, AFNOR (2012).

[58] F. Hunkeler, The resistivity of pore water solution- a decisive parameter of rebar corrosion and repair methods, Construction and Building Materials 10 (5) (1996) 381-389.

[59] S. Bonnet, F. Schoefs, M. Salta, Sources of uncertainties for total chloride profile measurements in concrete: quantization and impact on probability assessment of corrosion initiation, European Journal of Environmental and Civil Engineering (2017). http://dx.doi.org/10.1080/15732479.2017.1377737